

Robotic Perception-motion Synergy for Novel Rope Wrapping Tasks

Zhaoyuan Ma and Jing Xiao¹

Abstract—This paper introduces a novel and general method to address the problem of using a general-purpose robot manipulator with a parallel gripper to wrap a deformable linear object (DLO), called a rope, around a rigid object, called a rod, autonomously. Our method does not require prior knowledge of the physical and geometrical properties of the objects but enables the robot to use real-time RGB-D perception to determine the wrapping state and feedback control to achieve high-quality results. As such, it provides the robot manipulator with the general capabilities to handle wrapping tasks of different rods or ropes. We tested our method on 6 combinations of 3 different ropes and 2 rods. The result shows that the wrapping quality improved and converged within 5 wraps for all test cases.

Index Terms—Perception for Grasping and Manipulation, Perception-Action Coupling, Reactive and Sensor-Based Planning, Bimanual Manipulation, Sensor-based Control

I. INTRODUCTION

Manipulating flexible wire, cable, rope, or other DLOs has a wide range of applications, such as catheter inserting [1], surgical suturing [2], automotive [3], aerospace [4], electromechanical industries [5], and so forth. The deformable property results in high-dimensional state space for modeling DLO, which makes manipulating DLO challenging.

Existing research for handling DLOs is focused on robot motion planning for such basic tasks as tying/untying knots [6], [7], [8], forming a given shape [9], contact-based cable routing [10], inserting string and rope in a hole [11], and winding [12], [13]. While most of the research about DLO considers quasistatic manipulation, some also address dynamic manipulation [7], [13], [14].

Solving a DLO manipulation task usually contains three key steps: perception, modeling, and motion planning. Computer vision is often used to perceive a DLO's state. Some researchers attach AR tags along a wire harness as sampling points to detect deformation [3]. More generally, classic algorithms, such as uniform thresholding and Canny edge detector, are applied to extract cables in a controlled environment [10]. With the development of neural networks, deep learning is used to extract features of a DLO [9], [15]. Tactile servoing is another approach for DLO manipulation. She *et al.* design a gripper with GelSight for cable following and cable insertion tasks [16].

Common DLO modeling is done topologically or geometrically. Topology is helpful to describe the spatial relation of a DLO fragment in a knotting task, such as presented in Wakamatsu's work [8]. Different geometric methods are

broadly used for other types of tasks, for example, thin plate splines [2], parameterized curve with minimum energy-based scheme [4], multi-link system [7]. A bi-directional long short-term memory (LSTM) is also used to model the structure of a chain-like mass-spring system [9]. Alternatively, it is possible to bypass the modeling step with deep learning to create low-level joint control directly from input sensor data, as suggested by Suzuki *et al.* [6], who used a convolutional auto-encoder (CAE) and LSTM structure. The system used RGB images and proximity sensor information as input to generate robot joint angles directly.

Once the model is ready, a task-oriented motion planning method can be introduced to solve the problem, such as learning from demonstration [2], model predictive path integral (MPPI) control [9], planning based-on angular contact mobility index (ACMI) [10].

There are several papers investigating different aspects of DLO wrapping tasks. Lee *et al.* focused on testing the performance of simulating a high volume of possible contacts [17]. Göbert *et al.* [12] designed a customized end-effector to attach a winding filament to a cyclical mold with a rotation axis and planned the path of the mold.

Ito *et al.* studied using one whipping motion to wind a whip onto a target object with dynamic manipulation, rather than a quasistatic manner [13].

However, there is a lack of study to enable an off-the-shelf, general-purpose robot manipulator to perform general wrapping manipulation of a DLO around another object.

In this paper, we address the open problem of enabling a general-purpose robot manipulator with a simple parallel gripper to autonomously wrap a DLO around another object based on synergizing real-time perception and robot motion planning and control without requiring prior physical and geometrical information of both the rope and the rod. We are interested in providing a general robotic wrapping capability that can be applied to DLOs of varied materials, including different kinds of ropes, flexible cables, fibers, and so on. Specifically, the paper presents a novel approach for general-purpose robot wrapping operations with the following characteristics:

- It uses real-time perception of the objects and wrapping state to determine and adapt the robot motion for accomplishing and improving wrapping operations to achieve high-quality results.
- It re-uses and adjusts the canonical motion of making a single wrap of the DLO around the other object to be flexible to the length of the DLO (thus the length of the coil as the wrapping result) and to enable constant check and improvement of wrapping quality with feedback

¹The authors are with Dept. of Robotics Engineering, Worcester Polytechnic Institute, Worcester, MA 01609, USA {zma3, jxiaoz}@wpi.edu

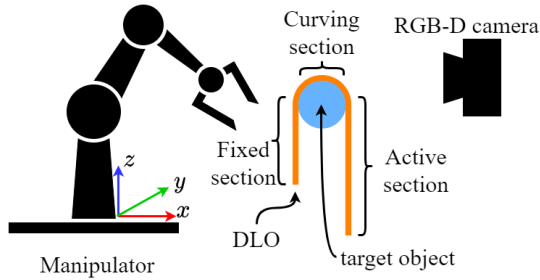


Fig. 1. The side view of the task setup.

control.

- Hence, it is able to achieve high-quality wrapping without requiring prior knowledge of the physical and geometrical properties of the DLO and the other object.

This paper is organized as follows. Section II defines the problem and setup. Section III introduces our approach in detail. Section IV describes our experiments and presents the results. Section V concludes the paper.

II. TASK DESCRIPTION

We define the task we study as wrapping a DLO, called the "rope", around a given rigid object, called the "rod". A coordinate system is set up at the base of the manipulator. The positive directions along the x , y , and z axes are defined as "front", "left", and "up" respectively from the manipulator's perspective. The rod is set in front of the manipulator. The manipulator has a gripper installed as the end-effector. As the initial state, the rope rides over the rod. We divide the rope into three sections: the fixed section, the curving section, and the active section. The fixed section is attached to a fixture or held by the manipulator without moving during the wrapping. The curving section has already been wrapped around the rod. The active section has sufficient length to create a few more wraps. The system could only obtain information through an RGB-D camera set to face the rod and the manipulator. The side view of the setup is depicted in Fig. 1. The goal of the task is for the manipulator to wrap the rope around the rod to create a helix that is tight in both radial and axial directions. Neither the dimensions nor the materials of the rod and the rope are known to the robot system.

III. APPROACH

We set up a real environment according to the task, as shown in Fig. 2. A dual-arm manipulator (YuMi IRB 14000, ABB) is placed on a tabletop for the task. The fingers of the manipulator have been modified to have a 2.5mm wide 30mm long slot between two fingers when the gripper is fully closed. This allows the rope to slide in between while keeping the tension of the rope. A support structure is mounted in front of the manipulator to install the rod. An RGB-D camera (RealSense Depth Camera D415, Intel) is placed to face the manipulator. The manipulator and the camera are connected to a desktop computer as the controller.

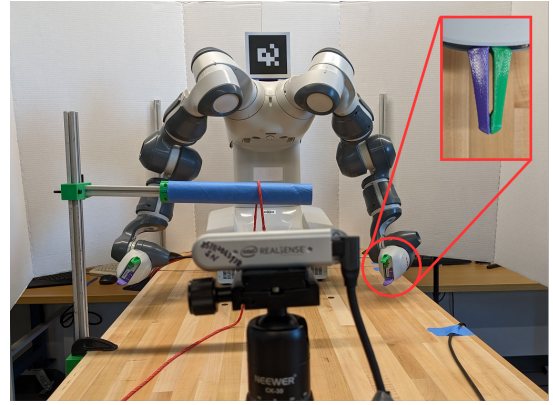


Fig. 2. The experiment setup.

Our approach is to enable the manipulator to learn how to make a high-quality helix of the rope around the rod by repeating and improving each single wrap along the helix.

Our system first conducts **rod estimation**: Using collected RGB images and point cloud data to estimate the position, orientation, and dimensions of the rod with respect to the manipulator automatically. This step is detailed in Section III-A.

Next, our system processes **rope estimation** by using RGB images and the rod estimation result to obtain the rope's color and diameter information. This step is described in Section III-B.

Subsequently, our system conducts a single wrap of the rope around the rod. It selects a point on the rope for grasping, moves the end-effector to grasp the point, executes the motion path to create one wrap, and releases the grip, which involves the following major procedures:

- 1) **Grasp point selection**: Using RGB images to search for a grasp point along the rope.
- 2) **Motion adjustment for wrapping**: Generating robot end-effector's wrapping motion path based on adjustable parameters.
- 3) **Auxiliary motion generation to facilitate wrapping**: Generating picking and releasing motions for the manipulator to perform before and after the wrapping motion respectively to complete the whole process.
- 4) **Motion outcome estimation and feedback control**: Using RGB images to estimate the outcome of the motion and adjust the parameters of the motion path generator.

Those procedures are described in Sections III-C to III-F in detail.

Our system repeats the single-wrap process above to generate a helix while improving the wrapping quality until the remaining rope is not sufficient for more wraps.

We enable the manipulator to continue practicing wrapping by unraveling the rope manually and letting the manipulator repeat the whole process until it can produce a tight helix wrap satisfactorily.

A. The rod estimation

Rod estimation is done as the first step of the whole process.

This process starts with establishing the transformation between the camera and the robot by using the RGB image from the camera and a fiducial marker [18] attached to the robot. The RGB-D camera provides a colorized depth map of the workspace (Fig. 3a). Let P denote the set of all the 3D points in the map, and let Q be the set of all 2D pixels with color information in the map. Each data point within the frame can be represented as $(p_x, p_y, p_z, q_x, q_y, c)$, where $(p_x, p_y, p_z) \in P$ is the position in the camera coordinate system, $(q_x, q_y, c) \in Q$ is the pixel location on the image plane, and c is the color.

Next, from the point cloud data captured by the camera, our system extracts the points between the robot and the camera, and above the tabletop. The system downsamples the extracted point cloud and applies DBSCAN [19] to create clusters according to the distance from the camera. An example result is shown as Fig. 3b. As there is no other object between the camera and the rod, the cluster with the shortest distance is selected. A 3D bounding box is created around this cluster (Fig. 3c). All points within the 3D bounding box are collected. White pixels in Fig. 3d indicate the selected data points in the 2D image plane. Those points are further classified into 2 clusters according to their hue with K-mean [20]. The cluster with the most data points is kept. A maximum inscribed rectangle is used to fit the kept points, as shown in Fig. 3e.

Finally, the points within the rectangle are treated as points on the rod, with $P' \subset P$ being the 3D points and $Q' \subset Q$ denoting the pixels. P' are used to estimate the radius r_{rod} and the length l_{rod} of the rod. Our system creates a half-cylinder surface template based on the estimation and employs ICP [21] to match it to P' (Fig. 3f). At this point, the estimates of the rod's center position $(x_{rod}, y_{rod}, z_{rod})$, the rod's orientation, and r_{rod} are obtained.

B. The rope estimation

Once the rod's information is determined, our system estimates the color (hue range) and the diameter d of the rope using Q' (highlighted by the red rectangle in Fig. 4a). It extracts the hue channel of Q' to create a histogram. Otsu's method [22] is applied to the histogram to find a threshold that can separate Q' into the rope and the rod. Then a Gaussian function $N(\mu, \sigma)$ is used to approximate the normalized rope's hue histogram. The hue range of the rope is chosen as $[\mu - 3\sigma, \mu + 3\sigma]$.

The hue threshold found above is also applied to Q' to create a binary mask of the rope. The result is shown as in Fig. 4b. A minimum area rectangle is generated to enclose the selected area, as in Fig. 4c. The short edge of the rectangle for the rope segment is taken as d .

C. Grasp point selection

Wrapping a rope typically requires grasping both the fixed section and the active section and moving the active one

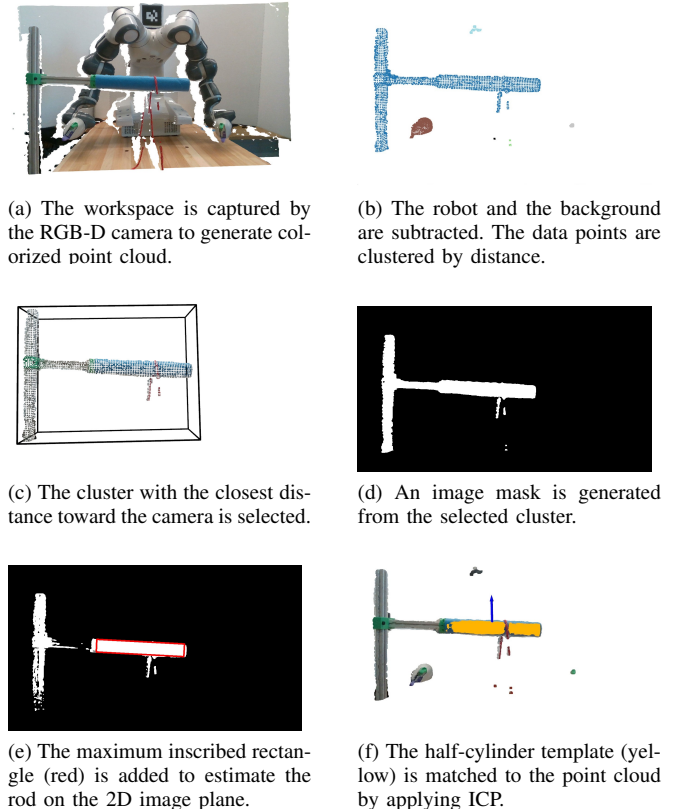


Fig. 3. Key steps to estimate the rod's dimension and pose.

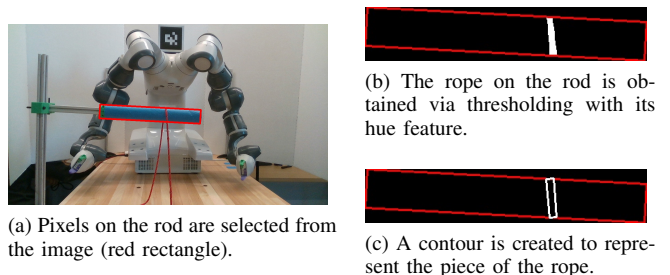


Fig. 4. Estimate the rope's width and color.

around the rod. Finding the grasp points on the two sections is performed with an unwrapped rope. For each additional wrapping motion, only the grasp point on the active section needs to be updated. The camera's limited 3D resolution makes it difficult to detect thin features, such as the rope, with the point cloud data. Therefore, this process is done based on the 2D RGB image.

Grasp point selection starts with extracting the two sections of the rope from the image. A sub-image of Fig. 4a is created as shown in Fig. 5a, by extending the bounding box of the rod at both sides and downward. The system employs Ariadne+'s [15] pre-trained DeepLabV3+ [23] to create a binary mask M_1 from the sub-image. Compared to traditional computer vision methods, this deep learning approach suggests possible rope areas with less noise. However, we observed that extraction defects may happen. For

example, Fig. 5b shows an incomplete detection on the fixed section that is near the rod. Therefore, our system applies the rope's hue range as the threshold to the sub-image to create another binary mask M_2 , as shown in Fig. 5c. M_2 is used to connect detected rope segments in M_1 as much as possible. For a white pixel in M_1 , if M_2 has a vertical white line segment across the pixel at the same position, all the pixels on this line are added to M_1 . The updated M_1 is then skeletonized [24] to reduce detected objects to 1-pixel width, as shown in Fig. 5d. Finally, our system searches for all lines from the bottom of the skeletonized mask, extracts the two longest lines, and calculates their center. The one near the right gripper (based on the robot's view) is taken as the fixed section (highlighted with green), and the one near the left gripper is taken as the active section (highlighted with blue), see Fig. 5e.

After the two sections of the rope are detected, our system determines one point along each of the sections for grasping by providing a value l_{gp} (in millimeters) measured from the lower edge of the rod. We assume: 1) both sections of the rope (within the image) are always parallel to the YZ plane (Fig. 1) and tangent to the rod, and 2) the distance between any two pixels and their distance in 3D are uniformly scaled. Our system converts l_{gp} to the measurement in pixels and searches the corresponding point along designated rope section. In Fig. 5e, the resulting point in the image plane is represented by a red dot. The position information of the pixel is converted back to the world coordinate system and used to move the robot's end-effector, as shown in Fig. 5f.

D. Motion adjustment for wrapping

The wrapping motion is the most crucial as it determines the quality of the generated wrapping helix. It is performed in the presence of the estimation error or uncertainty of the rod's pose, dimension, the grasp points along the rope, and the unknown physical properties of the rope.

Our approach is to create a spiral curve with just a few parameters for the robot end-effector to follow and then adjust the parameter values based on perception feedback. The goal is to achieve a resulting wrapping motion that can overcome the estimation errors and achieve a high-quality wrap in spite of the unknown physical properties of the rope.

To design the canonical spiral curve for the robot's end-effector, we assume a rope hangs over the rod naturally due to gravity, creating contact with the rod on the upper half of the cylinder and leaving the surface of the rod tangentially at points A and B , as shown in Fig. 6a. Let O be the center of the rod's cross-section where the rope lies. For the convenience of deriving the spiral function, we define a new 2D coordinate system with the origin at O and the x and y axes as indicated in Fig. 6a on the cross-section. The 3D coordinates of O can be obtained from their relation to the rod's center.

The fixed section starts from point A , extends downwardly, and is held by the robot's right gripper. The active section is extended from point B to the grasp point (x_0, y_0) , with the length L . We define $R = r_{rod} + \epsilon$, where ϵ is a variable

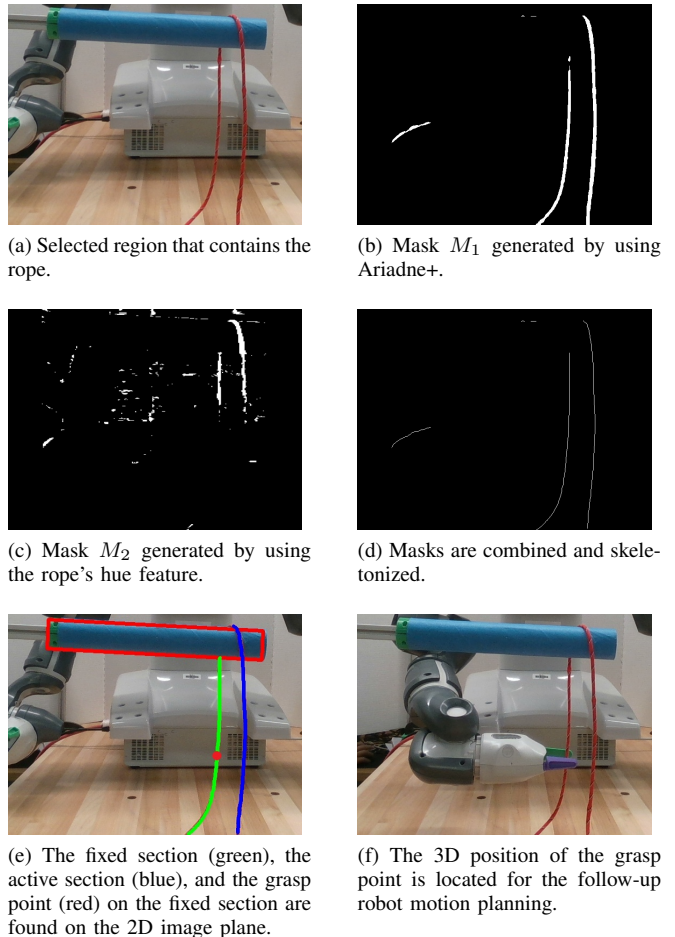
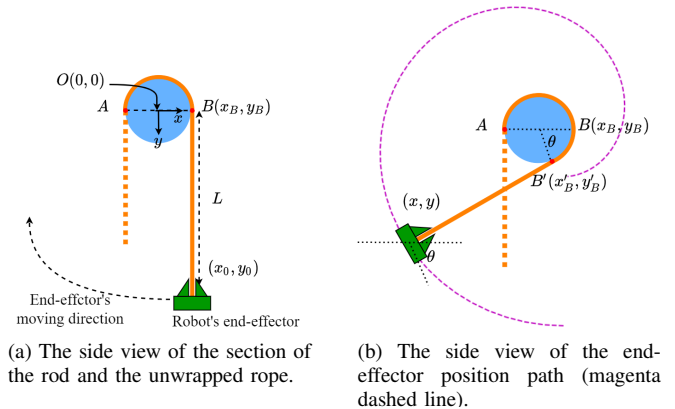
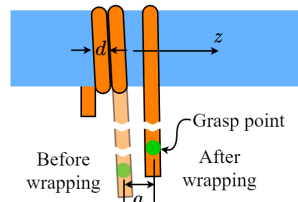


Fig. 5. Example of grasp point selection for the fixed section.



(a) The side view of the section of the rod and the unwrapped rope.

(b) The side view of the end-effector position path (magenta dashed line).



(c) The front view of the rope's diameter and the wraps' advance. The translucent orange section indicates the active section before the wrapping. The opaque one on its right is after wrapping.

Fig. 6. Spiral curve for the robot end-effector.

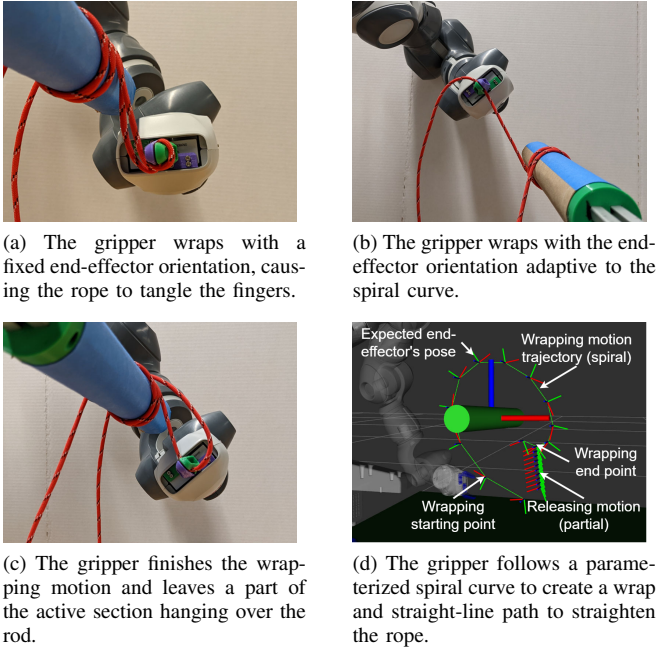


Fig. 7. The wrapping motion.

for correcting the estimation error in r_{rod} . We define $L = 2\pi R + L'$, where L' is a safe distance that considers the end-effector's size. Once the left gripper starts to make a wrap, the tangential contact point B moves to B' . Note that the wrapping angle $\theta \in [0, 2\pi]$ is the angle $\angle B'OB$. As an additional $\widehat{BB'} = \theta R$ of the rod is covered by the rope, the distance between the gripper to the tangential point B' is reduced to $L - \theta R$, as shown in Fig. 6b.

Now we consider the following spiral curve with respect to the rod coordinate system:

$$\begin{cases} x = R \cos \theta - (2\pi R + L' - \theta R) \sin \theta \\ y = R \sin \theta + (2\pi R + L' - \theta R) \cos \theta \\ z = a\theta/2\pi \end{cases} \quad (1)$$

where a is the displacement of the end-effector along the rod's axial direction for one wrap (Fig. 6c), which can be decided through feedback (see Section III-F). The 2D projection of this spiral path for the end-effector is shown as the magenta dashed curve in Fig. 6b.

Our system searches for the safety distance $L' \in [L'_{min}, L'_{max}]$ so that the wrapping path has a feasible inverse kinematics (IK) solution.

Note that the goal of the wrapping is to create wraps that are tight along the radial and axial directions of the rod, such that the wrap along the radial direction is as close to the radius of the rod as possible, and the distance along the axial direction from the center of two adjacent wraps equal to the diameter of the rope.

During the wrapping process, when the wrapping angle changes to θ , the end-effector rotates to the same angle θ about the rod's axis simultaneously, as indicated by its orientation in Fig. 6b. Without this rotation, the rope tends to entangle the fingers and hinder the gripper's opening motion

at the end of the wrap, as shown in Fig. 7a. The results of wrapping with the change of the end-effector orientation are shown in Fig. 7b ($\theta = 120^\circ$) and Fig. 7c ($\theta = 330^\circ$). At this stage, the position and orientation of the robot gripper along the spiral path have been determined with respect to the rod coordinate system, which can be converted to the world coordinate system.

In practice, our system takes samples along the spiral curve and discards the first and the last sampled points ($\theta = 0$ and 2π) to specify the end-effector wrapping motion. The wrapping motion is connected with auxiliary motions to prepare the rope for wrapping and to release it after wrapping, as detailed in Section III-E. Fig. 7d illustrates the connection of the wrapping motion to the releasing motion.

E. Generation of auxiliary motions to facilitate wrapping

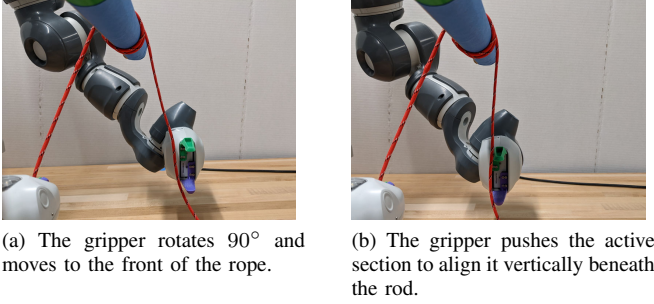
Rope picking and releasing motions are defined based on the spiral wrapping motion. Picking is a point-to-point motion that contains three key poses: 1) the entry pose, where the end-effector moves to the point with the opening of the gripper facing toward the rope at a distance. 2) the grasp pose, where the rope is squeezed in between the fingers of the gripper, and 3) the connection pose, where the gripper moves to the starting point of the spiral path. The grasp pose is derived as in Section III-C with L being the input value for l_{gp} . The entry pose is obtained by offsetting the grasp pose to move the end-effector away from the rope.

The release motion is designed to straighten the rope and to move the gripper away from the rope to avoid occlusion for image processing after the wrapping motion is done. Straightening the rope happens after the gripper arrives at the last sampled point of the spiral (see Fig. 7c and 7d). The gripper moves downward to follow a straight-line path, sliding along the rope to flip the active section to the front. Then the gripper releases the rope and withdraws to be away from the rope. At this point, if the remaining length of the active section is longer than the rod's height, part of the section may land on the table, preventing the rope drops vertically from the rod. An additional rope alignment step is added. The left gripper rotates 90° to increase the contact area with the rope. Then it moves to the front of the active section, as shown in Fig. 8a and pushes the rope towards the manipulator to ensure that the rope is roughly vertical beneath the rod (Fig. 8b). Finally, the gripper moves away from the rope to leave space for the next grasp point selection step.

F. Motion outcome estimation and feedback control

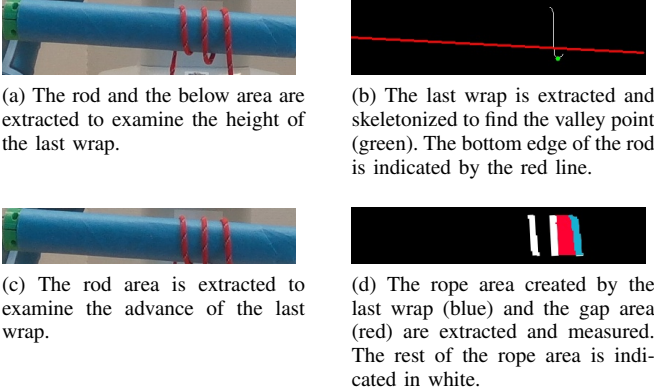
Following the completion of one wrap, our system takes an image of the result and checks for the tightness along the radial direction (refer to as the height) and the axial direction (refer to as the advance) of the wrap, which is then used for feedback control to improve the next wrap.

It starts by checking the height of the last wrapped part of the rope. At this step, a rectangle that contains the rod and some areas below is extracted from the image to include pieces of rope that could possibly hang under the rod, as



(a) The gripper rotates 90° and moves to the front of the rope. (b) The gripper pushes the active section to align it vertically beneath the rod.

Fig. 8. The auxiliary motions.



(a) The rod and the below area are extracted to examine the height of the last wrap. (b) The last wrap is extracted and skeletonized to find the valley point (green). The bottom edge of the rod is indicated by the red line. (c) The rod area is extracted to examine the advance of the last wrap. (d) The rope area created by the last wrap (blue) and the gap area (red) are extracted and measured. The rest of the rope area is indicated in white.

Fig. 9. Image processing to examine the motion outcome of the last wrap.

shown in Fig. 9a. The rope is extracted from the image by using the rope’s hue range as the threshold. Assuming that the rope segments in this binary image share the same width d as the detected rope’s diameter, our system searches the image for the rope segment created by the last wrap. The segment is skeletonized to find the valley point along it, as shown in Fig. 9b. The pixel distance from this point to the bottom of the rod is taken as the height feedback of the last wrap, noted as h . This feedback is used to estimate the radius R .

The feedback controller updates the R by:

$$R_{n+1} = R_n - K_{PR}(q_r), \text{ where } q_r = h - t_R \quad (2)$$

where K_{PR} is the proportional coefficient, t_R is a threshold. The stop condition is when $h \leq t_R$.

The RGB image is also used to check the advance. Pixels of the rod’s area (Fig. 9c) are selected and processed to extract the rope. The rope area created by the last wrap S_r and the gap between the last two wraps S_g are measured, as in Fig. 9d. The feedback controller updates the a by:

$$a_{n+1} = a_n - K_{Pa}(q_a), \text{ where } q_a = S_g / (S_g + S_r) \quad (3)$$

where K_{Pa} is the proportional coefficient. There are two stop conditions for learning the advance: 1) $q_a = 0$, 2) for two consecutive wraps n and $n + 1$, $|q_{an} - q_{a(n+1)}| < t_a$, where t_a is a threshold. When the wrapping output meets either condition, the system stops to update the advance.

IV. EXPERIMENTS AND RESULTS

In this section, we describe our experiments to implement and test our approach described in Section III and present the results. We then discuss the performance and potential improvement of the wrapping algorithm.

A. Experiment setup

The PC of our system is equipped with an Intel Core i5-7500, 16GB RAM, and an NVIDIA GeForce GTX 1050 Ti, running Ubuntu 20.04 with ROS Noetic. We modified KTH’s YuMi package [25] in order to control the manipulator. The YuMi is configured to run in manual mode, with 100% speed. Its Axis 6, where the gripper is mounted, has the ability to rotate from -229° to 229° , which is capable of a 360° continuous rotation mentioned in Section III-D. To achieve the required gripper motion during the wrapping, Axis 6 of the left arm was set to 216° at the beginning of wrapping and was at -144° when finished. Trac-IK [26] was used to calculate joint variables of the rest of the 6 axes of the left arm and the 7 axes of the right arm from expected end-effector poses. The solving timeout and the error toleration of this solver were set to 50ms and 1mm, respectively.

The coefficients of the feedback control in our system are given in Table I. The threshold t_R was set to $1.5d$ and t_a was set to 5%. The system’s advance feedback started with the initial $a_0 = 20\text{mm}$. For a rod with an estimated radius r_{rod} . The initial R was set to $1.5r_{rod}$. In practice, with a larger R , some waypoints of the spiral path may lie outside the manipulator’s workspace, which prevents the manipulator from executing the path. If this happens, R is reduced by a small value, which we set to 5mm in the experiments, to generate a new spiral path. This process repeats until the manipulator is able to follow the path to get height feedback for the first time. Then the system uses feedback control to tune R .

To validate the capability of handling objects with unknown attributes, we tested our system on two cylindrical rods and three ropes, namely Rod1, Rod2, Rope1, Rope2, and Rope3. Two rods share the same length of $l = 280\text{mm}$ but have different radii. The ground truth and the estimated radius of each rod can be found in Table II. For each rod, we ran the estimation 10 times. Rope1 is a skein of yarn (Softee Chunky Solid Yarn, Bernat). Rope2 is also a skein of yarn (Chenille Home Yarn, Loops & Threads). Rope3 is a skein of paracord (1/8 in. x 50 ft. Assorted Color Paracord, Everbilt). We tested our system on the 6 combinations of the rods and ropes.

B. Wrapping outcome

We used one estimated radius r_{rod} for each rod to examine the wrapping algorithm. The system uses the method mentioned in Section III-D to obtain R and L' . We find that the system’s selection of the values of these two parameters is independent of the ropes. These parameter values are shown in Table III.

The robot took 5 trials to reach the stop condition for learning the advance in the axial direction for {Rod1,

TABLE I
THE COEFFICIENTS OF THE FEEDBACK CONTROL

L'_{\min}	L'_{\max}	K_{PR}	K_{Pa}
20mm	60mm	0.001	0.04

TABLE II
THE GROUND TRUTH AND THE ESTIMATION OF r_{rod} (OVER 10 TIMES).

	Ground truth	Estimation average (Standard deviation)	Range
Rod1	21mm	18.5(± 1.8)mm	17.4 ~ 20.7mm
Rod2	17mm	14.3(± 1.1)mm	13.6 ~ 14.6mm

Rope3}, {Rod2, Rope1}, and {Rod2, Rope3}. For {Rod1, Rope1} and {Rod1, Rope2}, it took 3 trials. It achieved the axial tightness in the first trial for {Rod1, Rope2}. The result can be found in Table IV. These images were taken by the RGB-D camera and were also used for the feedback control process. Note that since Rope3 has a higher stiffness, making the first wrap tends to push the fixed section to create a larger gap compared to the following wraps (see Fig. 10). This only happens to Rope3 when no previous wrap is made. Therefore, we always kept one pre-wrap on the rod that was not taken into account when testing Rope3 on both rods.

For all cases, the tightness along the radial direction was met. For cases with Rope1 and Rope2, the axial tightness was also met. For cases with Rope3, the final result was comparable with the wrapping result by a person manually

TABLE III
THE PARAMETERS THAT THE SYSTEM CHOSE TO ACHIEVE RADIAL TIGHTNESS.

	Estimated radius r_{rod}	R	L'
Rod1	20.7mm	21.0mm	60.0mm
Rod2	14.6mm	16.9mm	60.0mm

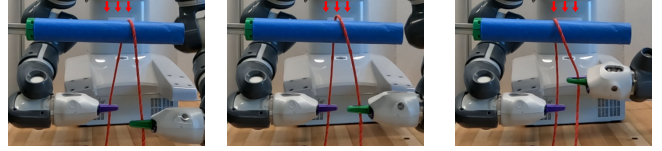


Fig. 10. The fixed end of the Rope3 is shifted during creating the first wrap because of its' stiffness. The red arrows are used as references.

(see the last column of Table IV).

The attached video shows the robot performing those wrapping cases.

C. Time efficiency analysis

We report the time consumption of our method in two parts: the computation time and the total execution time. The computation time includes all the calculation steps that are described in Section III. The total execution time counts the computation time and the manipulator executing the picking, wrapping, and releasing motions described in Sections III-D and III-E.

For the computation time, we repeat each step 10 times to evaluate the average and standard deviation of the running time. Our system spends 13.197(± 0.402)s to finish the rod estimation and 1.042(± 0.053)s to finish the rope estimation at the beginning of a wrapping task. These are the pre-processing steps before wrapping and only need to be done once for each combination. The average time consumption of steps to conduct a single wrap can be found in Table V. The motion planning time in the table is the total time of planning for wrapping and auxiliary motions, which includes solving IK and polynomial interpolation in the joint space.

TABLE V
AVERAGE COMPUTATION TIME OF STEPS TO CONDUCT A SINGLE WRAP.

Step	Time (sec)
Grasp point selection	4.447(± 0.082)
Motion planning	2.302(± 0.050)
Motion outcome estimation	0.312(± 0.016)

TABLE IV

WRAPPING OUTCOME OF EACH CASE. THE NUMBERS ABOVE THE WRAPS INDICATE THE TRIAL NUMBER. a_i IS THE CORRESPONDING ADVANCE THAT IS USED TO ACHIEVE THAT WRAP.

	Rope1		Rope2			Rope3			Human wrapping	
Rod1										 Wrapping performed by hands as a comparison.
	$a_1 = 20.0$ $a_2 = 11.2$	$a_3 = -2.7$ (complete)		$a_1 = 20.0$ (complete)			$a_1 = 20.0$ $a_2 = 2.4$	$a_3 = -11.8$ $a_4 = -18.1$	$a_5 = -21.0$ (complete)	
Rod2										
	$a_1 = 20.0$ $a_2 = 10.3$	$a_3 = 9.7$ $a_4 = 6.0$	$a_5 = 4.7$ (complete)	$a_1 = 20.0$	$a_2 = 17.3$	$a_3 = 17.0$ (complete)	$a_1 = 20.0$ $a_2 = 0.1$	$a_3 = -7.3$ $a_4 = -7.4$	$a_5 = -11.2$ (complete)	

We also measure the total execution time (including computation and movement time) of one wrap 10 times for {Rod1, Rope1}. The average time and the standard deviation is 63.933(± 0.611)s, which is an order of magnitude higher than the computation time for planning the wrap and auxiliary motion.

D. Discussion

We have observed that the radial feedback meets the stop condition from the first wrap for all test cases. Due to the camera's perspective and the methods mentioned in Section III-A, the estimated r_{rod} is always smaller than the ground truth. With R being less or equal to the ground truth, the gripper slid slightly down the active section of the rope during the wrapping to compensate for the insufficient rope length from the gripper to the rod. This motion keeps the tension of the section and results in radial tightness. This suggests that to wrap over a solid of revolution, an R that is smaller than the ground truth can be tolerated and often helpful for radial tightness.

V. CONCLUSIONS

In this paper, we present a novel and general method to solve the problem of using a general-purpose robot manipulator with a parallel gripper to wrap ropes around a rigid rod. This method is based on a parameterized canonical motion and does not require knowledge of the rope or the rod. It uses RGB-D images to estimate the state of the rope and rod, evaluates the wrapping outcome, and generates feedback from the outcome to improve motion planning. We tested our method with 6 combinations of ropes and rods. The result shows that our general method applies to different ropes and rods very well. In the next step, we will expand to using other types of rods, for instance, solids of revolution other than cylinders, such as a cone, and to incorporate tactile sensing.

REFERENCES

- [1] J. Jayender, R. Patel, and S. Nikumb, "Robot-assisted catheter insertion using hybrid impedance control," in *Proc. IEEE Int. Conf. Robot. Autom.*, 2006, pp. 607–612.
- [2] J. Schulman, A. Gupta, S. Venkatesan, M. Tayson-Frederick, and P. Abbeel, "A case study of trajectory transfer through non-rigid registration for a simplified suturing scenario," in *Proc. IEEE/RSJ Int. Conf. Intell. Robots Syst.*, 2013, pp. 4111–4117.
- [3] X. Jiang, K.-m. Koo, K. Kikuchi, A. Konno, and M. Uchiyama, "Robotized assembly of a wire harness in car production line," in *Proc. IEEE/RSJ Int. Conf. Intell. Robots Syst.*, 2010, pp. 490–495.
- [4] A. Shah, L. Blumberg, and J. Shah, "Planning for manipulation of interlinked deformable linear objects with applications to aircraft assembly," *IEEE Trans. Autom. Sci. Eng.*, vol. 15, no. 4, pp. 1823–1838, 2018.
- [5] J. Franke and A. Dobroschke, "Robot-based winding-process for flexible coil production," in *Proc. Elect. Manufact. Tech. Conf.*, 2009, pp. 157–163.
- [6] K. Suzuki, M. Kanamura, Y. Suga, H. Mori, and T. Ogata, "In-air knotting of rope using dual-arm robot based on deep learning," in *Proc. IEEE/RSJ Int. Conf. Intell. Robots Syst.*, 2021, pp. 6724–6731.
- [7] Y. Yamakawa, A. Namiki, and M. Ishikawa, "Motion planning for dynamic knotting of a flexible rope with a high-speed robot arm," in *Proc. IEEE/RSJ Int. Conf. Intell. Robots Syst.*, 2010, pp. 49–54.
- [8] H. Wakamatsu, E. Arai, and S. Hirai, "Knotting/un-knotting manipulation of deformable linear objects," *Int. J. Robot. Res.*, vol. 25, no. 4, pp. 371–395, 2006.
- [9] M. Yan, Y. Zhu, N. Jin, and J. Bohg, "Self-supervised learning of state estimation for manipulating deformable linear objects," *IEEE Robot. Autom. Lett.*, vol. 5, no. 2, pp. 2372–2379, 2020.
- [10] J. Zhu, B. Navarro, R. Passama, P. Fraisse, A. Crosnier, and A. Cherubini, "Robotic manipulation planning for shaping deformable linear objects with environmental contacts," *IEEE Robot. Autom. Lett.*, vol. 5, no. 1, pp. 16–23, 2020.
- [11] W. Wang, D. Berenson, and D. Balkcom, "An online method for tight-tolerance insertion tasks for string and rope," in *Proc. IEEE Int. Conf. Robot. Autom.*, 2015, pp. 2488–2495.
- [12] A. Göbert, A. Deetman, A. Rossi, O. Weyhe, and P. Eversmann, "3dwoodwind: robotic winding processes for material-efficient lightweight veneer components," *Constr. Robot.*, vol. 6, no. 1, pp. 39–55, 2022.
- [13] Koichiro Ito, Y. Yamakawa, and M. Ishikawa, "Winding manipulator based on high-speed visual feedback control," in *2017 IEEE Conf. Control Technol. Appl. (CCTA)*, 2017, pp. 474–480.
- [14] H. Zhang, J. Ichnowski, D. Seita, J. Wang, H. Huang, and K. Goldberg, "Robots of the lost arc: Self-supervised learning to dynamically manipulate fixed-endpoint cables," in *Proc. IEEE Int. Conf. Robot. Autom.*, 2021, pp. 4560–4567.
- [15] A. Caporali, R. Zanella, D. De Gregorio, and G. Palli, "Ariadne+: Deep Learning-based Augmented Framework for the Instance Segmentation of Wires," *IEEE Trans. Ind. Inform.*, pp. 1–1, 2022.
- [16] Yu She, S. Wang, S. Dong, N. Sunil, A. Rodriguez, and E. Adelson, "Cable manipulation with a tactile-reactive gripper," *Int. J. Robot. Res.*, vol. 40, no. 12-14, pp. 1385–1401, 2021.
- [17] J. Lee, M. Lee, J. Yoon, and D. Lee, "A parallelized iterative algorithm for real-time simulation of long flexible cable manipulation," in *Proc. IEEE Int. Conf. Robot. Autom.*, 2021, pp. 12 040–12 046.
- [18] ar_track_alvar. [Online]. Available: http://wiki.ros.org/ar_track_alvar
- [19] M. Ester, H.-P. Kriegel, J. Sander, and X. Xu, "A density-based algorithm for discovering clusters in large spatial databases with noise," in *Proc. 2nd Int. Conf. Knowl. Discov. Data Min.*, 1996, pp. 226–231.
- [20] J. MacQueen, "Some methods for classification and analysis of multivariate observations," *Proc. 5th Berkeley Symp. Math. Stat. Probab., Vol. 1: Stat.*, vol. 5.1, pp. 281–298, 1967.
- [21] P. Besl and N. D. McKay, "A method for registration of 3-d shapes," *IEEE Trans. Pattern Anal. Mach. Intell.*, vol. 14, no. 2, pp. 239–256, 1992.
- [22] N. Otsu, "A threshold selection method from gray-level histograms," *IEEE Trans. Syst., Man, Cybern.*, vol. 9, no. 1, pp. 62–66, 1979.
- [23] L.-C. Chen, Y. Zhu, G. Papandreou, F. Schroff, and H. Adam, "Encoder-Decoder with Atrous Separable Convolution for Semantic Image Segmentation," in *Proc. Conf. Eur. Comput. Vis. (ECCV)*, 2018, pp. 833–851.
- [24] T. Y. Zhang and C. Y. Suen, "A fast parallel algorithm for thinning digital patterns," *Commun. of the ACM*, vol. 27, no. 3, pp. 236–239, 1984.
- [25] kth-ros-pkg/yumi. [Online]. Available: <https://github.com/kth-ros-pkg/yumi>
- [26] P. Beeson and B. Ames, "TRAC-IK: An open-source library for improved solving of generic inverse kinematics," in *2015 IEEE-RAS 15th Int. Conf. Humanoid Robots (Humanoids)*, 2015, pp. 928–935.